Inorganic Chemistry

Article

pubs.acs.org/IC

$K_2M^{III}_2(M^{VI}O_4)(PO_4)_2$ (M^{III} = Fe, Sc; M^{VI} = Mo, W), Novel Members of the Lagbeinite-Related Family: Synthesis, Structure, and Magnetic Properties

Nikolay S. Slobodyanik,[†] Kateryna V. Terebilenko,*[,†] Ivan V. Ogorodnyk,[†] Igor V. Zatovsky,[†] Maksym Seredyuk,[†] Vyacheslav N. Baumer,[‡] and Philipp Gütlich[§]

[†]Inorganic Chemistry Department, Kiev Taras Shevchenko University, Volodymyrska Street 64, Kiev 01601, Ukraine

[‡]STC Institute for Single Crystals NAS of Ukraine, 60 Lenin Avenue, Kharkiv 61001, Ukraine

[§]Institut für Anorganische und Analytische Chemie, Johannes-Gutenberg-Universität, Staudinger-Weg 9, D-55099 Mainz, Germany

Supporting Information

ABSTRACT: The possibility of PO_4^{3-} for MoO_4^{2-} partial substitution in the langbeinite framework has been studied by exploration of the K–Fe(Sc)–Mo(W)–P–O systems using the high-temperature solution method. It was shown that $1/3PO_4^{3-}$ for MoO_4^{2-} substitution leads to formation of three novel compounds $K_2Fe(MoO_4)(PO_4)_2$, $K_2Sc(MoO_4)(PO_4)_2$, and $K_2Sc(WO_4)(PO_4)_2$ with slightly increased lattice parameters and significant distortion of the anion tetrahedra without structure changes. In contrast, the antiferromagnetic structure is modified by substitution in the low-temperature region. The structural peculiarities are discussed in light of bond-valence sums calculations.

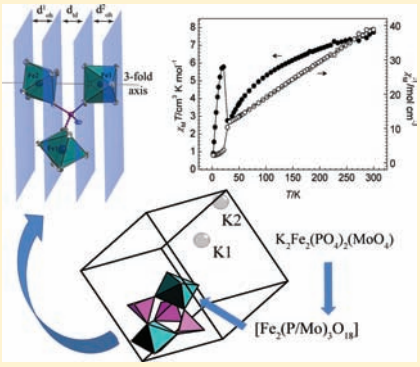

INTRODUCTION

Substitution of cationic or/and anionic sites is a common strategies in exploring the aria of materials with purely inorganic frameworks. For instance, a group of $ABOXO_4$ compounds (A = Li, Na, K, Rb, Cs; B = Ti, Zr, Hf, Ge, Sn; X = P, As, Si) with a parent compound $KTiOPO_4$ was successfully widened in both ways, however, mostly by uni- and aliovalent substitution within the cationic framework,[1,2] while there are very few examples of insertion into the rigid anionic network with other tetrahedral units, specifically AsO_4^{3-}, SiO_4^{4-}, or GeO_4^{2-}.[3,4] Replacement of structural fragments for $KTiOPO_4$-related compounds has been proved to influence not only the structural peculiarities but also the nonlinear optical properties.[5]

Some correlations between the degree of structural distortion provoked by substitution with changes in physical properties were found for magnetoresistant perovskites $ACu_3Mn_4O_{12}$ (A = Ca, La, Bi),[6] anode materials $MLi_2Ti_6O_{14}$ (M = Sr, Ba, 2Na),[7] and apatites $M_{10}(TO_4)_6X_2$ (M = alkaline earth, Pb, alkali, rare earth; T = P, As, Si, Ge, S, V, Cr, Mn; X = OH^-, halogen, $1/2O^{2-}$,$1/2CO_3^{2-}$) with interesting optical properties.[8] Thereby, deeper understanding of the substitution as well as its limits in addition to structure–function connectivity are necessary for further investigations of important inorganic materials.

Considering the fundamental possibility of different anions coexisting within the same framework we have taken a group of langbeinite-related compounds. To our knowledge, this group of general formula $A_xB_2(XO_4)_3$ (x = 1–2) has been paid much attention due to its complex phase transitions[9] and magnetic behavior.[10,11] Depending on the charge of anionic species XO_4^{n-} different polyvalent cations may complete the cationic position A. In the case of charge −2 (SO_4^{2-}, SeO_4^{2-}, CrO_4^{2-}, MoO_4^{2-}) the framework is built up mostly from divalent metals B (B = Mn, Mg, Cd, Ca, Ni, Co).[9] Within the structural type there are some exceptional representatives: a host lattice with "V_3O" clusters $K_{11}V_{15}P_{18}O_{73}$[12] and an "empty" lattice without alkaline metals $Pb_{1.5}V_2(PO_4)_3$[13] that shows a great ability of the langbeinite structure to adopt different cations.

The subject of our investigation is the coexistence of different anions with different charges in this framework. Taking into account that MoO_4^{2-} (WO_4^{2-}) anion takes divalent metals to form langbeinite structure while PO_4^{3-} prefers mostly tetravalent, superposition of both tetrahedral anions within the langbeinite framework should be observed in the case of applying trivalent cations: $M^{+2} + M^{+4} = 2M^{+3}$. Molten salt synthesis in the system $K_2M^{VI}O_4$–$M^{VI}O_3$–KPO_3–$M^{III}_2O_3$ (M^{III} = Fe, Cr, Sc; M^{VI} = Mo, W) was chosen as a suitable preparative approach to study the degree of possible substitution between both XO_4 groups and their interference. In this case the presence of different anionic salts may provide additional variety in the structural features of the products starting from minor doping and ending with formation of a

Received: July 26, 2011
Published: January 19, 2012

   dx.doi.org/10.1021/ic201575v | *Inorg. Chem.* 2012, 51, 1380–1385

unique structure, which contains both phosphate and molybdate groups.

Herein, phase relations in molten systems K−Fe(Sc)−Mo(W)−P−O and the growth and crystal structure of new langbeinite-related compounds $K_2M^{III}{}_2(M^{VI}O_4)(PO_4)_2$ (M^{III} = Fe, Sc; M^{VI} = Mo, W) are presented and discussed.

EXPERIMENTAL SECTION

Studies in Molten Systems K−M^{III}−M^{VI}−P−O (M^{III} = Fe, Cr, Sc; M^{VI} = Mo, W). In the first step of the investigation experiments were performed only in the cross-section $K_2M^{VI}{}_2O_7$−KPO_3 containing 5−20 mol % $M^{III}{}_2O_3$ (Cr, Sc, Fe) to adjust convenient molar ranges. For iron and scandium oxides 10 mol % was chosen as the most suitable content for more detailed investigation of the crystallization within a ternary system $K_2M^{VI}O_4$− $M^{VI}O_3$−KPO_3. The results of the investigation were shown on triangle diagrams $K_2M^{VI}O_4$−$M^{VI}O_3$−KPO_3 having $M^{III}{}_2O_3$ fixed to 10 mol %. Each point inside these diagrams (Figure 1−3) with coordinates ($xM^{I}{}_2M^{VI}O_4$; $yMoO_3$; $zM^{I}PO_3$) corresponds to a composition of a starting high-temperature solution $0.9xM^{I}{}_2MoO_4$ + $0.9yMoO_3$ + $0.9zM^{I}PO_3$ + $0.1M^{III}{}_2O_3$. Projections of crystallization fields on the composition diagram were constructed by taking into account results of phase analyses and pointing out areas with common solid content.

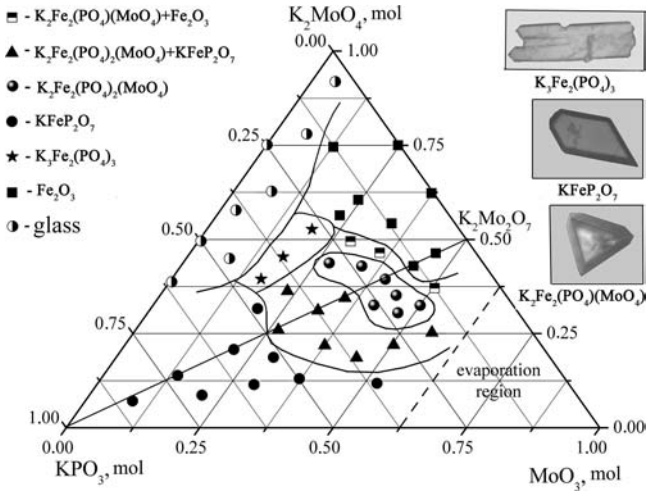

Figure 1. Phase relations in the K−Fe−P−Mo−O system with a Fe_2O_3 initial content of 10% mol.

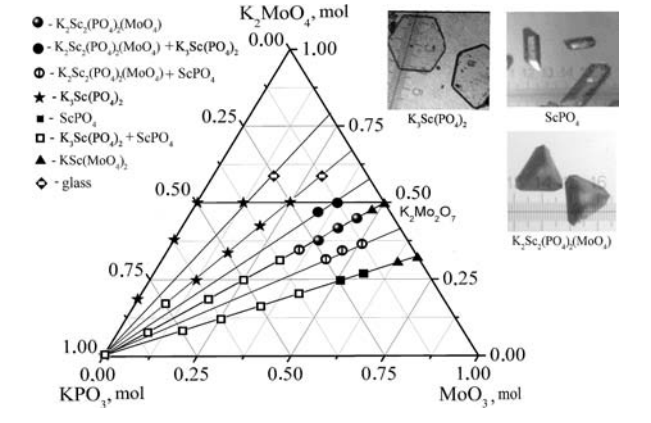

Figure 2. Crystallization products in the K−Sc−P−Mo−O molten systems with a Sc_2O_3 initial content of 10% mol.

Experiments were carried out using analytically pure K_2MoO_4, MoO_3, KPO_3, and $M^{III}{}_2O_3$ (M^{III} = Fe, Cr, Sc). Initial mixtures of calculated amounts of components were held at 1270 K for 2−3 h in platinum crucibles. High-temperature solutions obtained in this way were gradually cooled at a rate of 10−30 K/h from 920 to 820 K and, finally, poured out on a copper sheet. Crystalline products were retrieved from a solidified melt in hot distilled water. Then they were examined by optical microscopy, FTIR spectroscopy, and powder X-ray diffraction.

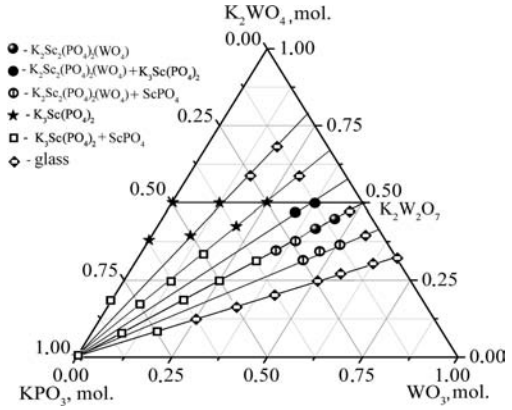

Figure 3. Composition diagram of the K−Sc−P−W−O systems with a Sc_2O_3 initial content of 10% mol with crystalline products indicated.

Single crystals of $K_2Fe_2(MoO_4)(PO_4)_2$ (KFeMo) were grown using the method described above by crystallizing a mixture of 6.40 g (0.027 mmol) of K_2MoO_4, 5.76 g (0.040 mmol) of MoO_3, 2.24 g (0.019 mmol) of KPO_3, and 1.60 g (0.01 mmol) of Fe_2O_3 to 910 K at a rate of 10 K/h.

Crystalline $K_2Sc_2(MoO_4)(PO_4)_2$ (KScMo) was prepared from a molten salt composition of 1.77 g of KPO_3, 1.14 g of Sc_2O_3, 14.28 g of K_2MoO_4, and 8.64 g of MoO_3 and $K_2Sc_2(WO_4)(PO_4)_2$ (KScW) from a mixture of 1.77 g of KPO_3, 1.14 g of Sc_2O_3, 17.11 g of K_2WO_4, and 16.37 g of WO_3 using the technique described above.

X-ray Diffraction and Structure Determination. Powder X-ray patterns were recorded at room temperature on a Shimadzu XRD-6000 diffractometer with Cu Kα radiation (λ = 1.5418 Å) to identify all phases and check the purity for each point inside the triangle. Some reference patterns from a database PDF2 were used to identify known crystal structures of $K_3Fe_2(PO_4)_3$ (PDF2 No.76-1628), Fe_2O_3 (PDF2 No. 80-2377), $KFeP_2O_7$ (PDF2 No. 89-1451), $KSc(MoO_4)_2$ (PDF2 No. 74-2009), $K_3Sc(PO_4)_2$ (PDF2 No. 78-0869), and $ScPO_4$ (PDF2 No. 84-0336). For novel compounds diffraction data were collected on a STOE IPDS-I diffractometer at 210 K using monochromatized Mo Kα radiation (λ = 0.71073 Å) for KFeMo and on an Oxford Diffraction XCalibur-3 diffractometer equipped with 4 MPixel CCD detector using monochromatized Mo Kα radiation (λ = 0.71073 Å) for KScMo and KScW. Structures were solved using direct methods by SHELXS-97[14] and refined in the full-matrix least-squares technique in the anisotropic approximation using the SHELXL-97[14] program packages. The ratio P/M^{VI} was constricted according to chemical analysis. Crystallographic data and structural refinements for three compounds are summarized in Table 1. Important bond distances are listed in Table 2.

Chemical Composition. ICP-AES (inductively coupled plasma-atomic emission spectroscopy) determination of K, Fe, Mo, and P amounts was performed on a "Spectroflame Modula ICP" ("Spectro", Germany) instrument. Elemental analysis showed similar results for this compound from different points obtained inside the corresponding area: K/Fe/Mo/P mole ratio is 1.96/0.98/1.04/1.98, which is in agreement with structural analysis. For KScMo and KScW elemental analysis has shown the K/Sc/Mo(W)/P mole ratio is 1.98/0.99/1.02/1.98 and 1.96/0.96/1.07/1.92

Mössbauer, IR Spectroscopy, and Magnetic Properties. The Mössbauer spectrum was recorded in transmission geometry with a ^{57}Co/Rh source kept at room temperature and a conventional spectrometer operating in the constant-acceleration mode. The samples were sealed in Plexiglas sample holders and mounted in a

dx.doi.org/10.1021/ic201575v | Inorg. Chem. 2012, 51, 1380−1385

Table 1. Crystallographic Data and Structure Refinement Parameters of $K_2M^{III}{}_2(PO_4)_2(M^{VI}O_4)$ (M^{III} = Fe, Sc; M^{VI} = Mo, W)

formula	$K_2Fe_2(PO_4)_2(MoO_4)$	$K_2Sc_2(PO_4)_2(MoO_4)$	$K_2Sc_2(PO_4)_2(WO_4)$
cryst syst	cubic	cubic	cubic
space group	$P2_13$	$P2_13$	$P2_13$
cell parameters a (Å)	10.0405(6)	10.3179(2)	10.3372(2)
V (Å^3)	1012.20(10)	1098.43(4)	1104.61(4)
Z	4	4	4
μ (mm^{-3})	5.252	3.425	12.685
T_{min}, T_{max}	0.605; 0.882	0.7214; 0.7683	0.2520; 0.4705
θ_{min}, θ_{max} (deg)	2.87; 25.41	3.42; 29.94	2.79; 29.96
R_{int}		0.0683	0.064
F(000)	1032	992	1120
R_1(all)	0.0408	0.0458	0.0444
wR_2	0.0868	0.0802	0.0522
S	1.304	0.969	1.083
no. of params	60	61	61
$\Delta\rho$, max; min (e Å^{-3})	0.683; −0,637	−0.399; 0.444	0.611; −0,667
Flack parameter	0.02(8)	0.18(9)	−0.01(2)

Table 2. Geometry of $P/M^{VI}O_4$ in (Å) for $K_2M^{III}{}_2(PO_4)_2(M^{VI}O_4)$ (M^{III} = Fe, Sc; M^{VI} = Mo, W)

P/Mo(1)−O(3)	1.561(7)
P/Mo(1)−O(4)	1.567(7)
P/Mo(1)−O(1)	1.572(8)
P/Mo(1)−O(2)	1.612(7)
P/Mo(1)−O(3)	1.566(6)
P/Mo(1)−O(2)	1.576(3)
P/Mo (1)−O(1)	1.579(1)
P/Mo(1)−O(4)	1.614(3)
P/W(1)−O(3)	1.573(6)
P/W(1)−O(4)	1.575(5)
P/W(1)−O(1)	1.585(5)
P/W(1)−O(2)	1.620(5)

nitrogen-bath cryostat. The Recoil 1.03a Mössbauer Analysis Software was used to fit the experimental spectra.

FTIR spectra were collected at room temperature in KBr disks using a Nicolet Nexus FTIR spectrometer at 400−4000 cm^{-1}.

Variable-temperature magnetic susceptibility measurements were recorded with a Quantum Design MPMS2 SQUID susceptometer equipped with a 7 T magnet, operating at temperatures in the range 2−400 K. The susceptometer was calibrated with metallic palladium. Measurements were performed on finely ground samples (15−30 mg). Magnetic data were corrected for the sample holder and diamagnetic contribution. Least-squares fitting of the experimental curves with the Curie−Weiss equation was performed with the program Origin 8.0.

RESULTS AND DISCUSSION

Crystallization Trends in K−M^{III}−M^{VI}−P−O (M^{III} = Fe, Cr, Sc; M^{VI} = Mo, W) Systems. At the first stage of the investigation the chromium-containing system was excluded from the following study due to a wide area of glass formation caused by Cr(III)−Cr(VI) redox reaction, whereas the K−Fe−W−P−O system revealed only vitreous products, detecting no crystalline product formed.

Taking into consideration a binary section KPO_3−$K_2M^{VI}{}_2O_7$ the areas of crystalline phases change gradually from phosphates ($K_3Sc(PO_4)_2$ and $K_3Fe_2(PO_4)_3$) through mixed phosphate−molybdate (tungstate) to pure molybdate (Figures 1−3). On the contrary, the role of the molybdate component in this section changes dramatically. Conventional application of K−Mo−O salts as an inert solvent corresponds to regions enriched in phosphates. As shown earlier, K_2MoO_4 or

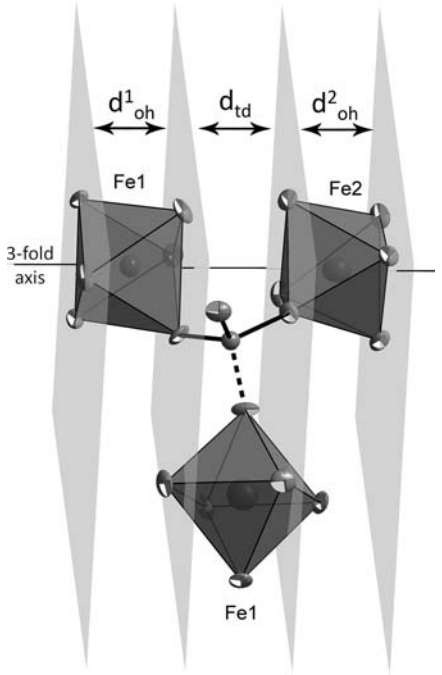

Figure 4. $[Fe_2(P/Mo)_3O_{18}]$ structural fragment with d values indicated.

$K_2Mo_2O_7$ addition to high-temperature solutions lowers the temperature and viscosity of the melt to originate phosphate solids[15] or create mild conditions for unique compounds synthesis that cannot be prepared from pure molten phosphates.[16] Both cases may be illustrated by the schemes

$$Fe_2O_3 + 3KPO_3 = K_3Fe_2(PO_4)_3$$

$$2K_2MoO_4 + Sc_2O_3 + 4KPO_3 = 2K_3Sc(PO_4)_2 + K_2Mo_2O_7$$

$$6KPO_3 + Fe_2O_3 = 2KFeP_2O_7 + K_4P_2O_7$$

Thus, the molybdate component either does not participate directly in phase formation or acts as an additional source of alkaline metal. When the concentration of the molybdate component ($K_2M^{VI}{}_2O_7$−$M^{VI}O_3$) reaches 75% mol it becomes

dx.doi.org/10.1021/ic201575v | Inorg. Chem. 2012, 51, 1380−1385

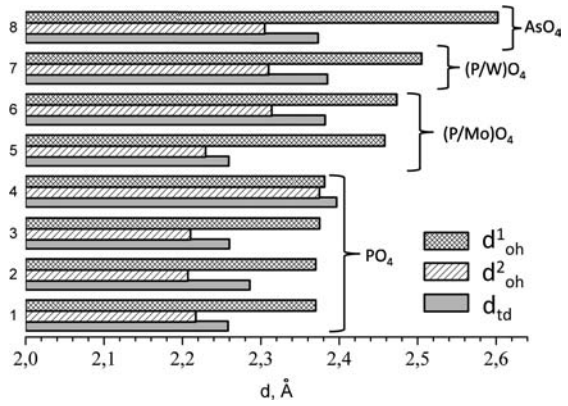

Figure 5. Comparison of d^1_{oh}, d^2_{oh}, and d_{td} calculated values for (1) $K_{1.84}Fe_{1.42}Nb_{0.58}(PO_4)_3$, (2) $K_2FeSn(PO_4)_3$, (3) $K_2Fe_{0.5}Ti_{1.5}(PO_4)_3$, (4) $Rb_2YTi(PO_4)_3$, (5) KFeMo, (6) KscMo, (7) KScW, and (8) $K_2ScSn(AsO_4)_3$.

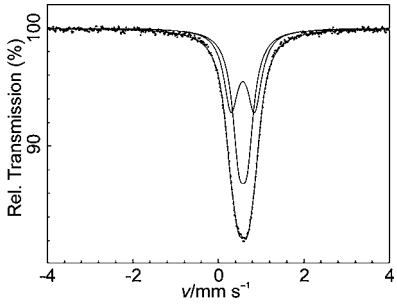

Figure 6. Mössbauer spectrum of KFeMo recorded at 80 K.

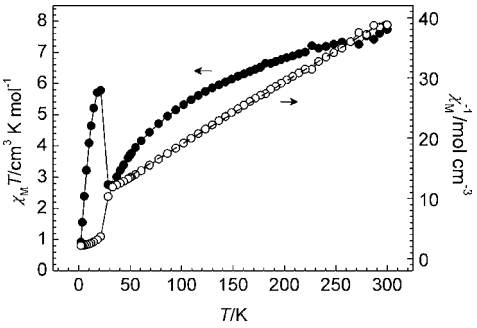

Figure 7. Plot of $\chi_M T$ and χ_M^{-1} versus T for KFeMo. The dashed line corresponds to fit to the data, as described in the text.

not only a reaction media but also a direct participant of interaction.

$$K_2M^{VI}{}_2O_7 + M^{III}{}_2O_3 + 2KPO_3 = K_2M^{III}{}_2(M^{VI}O_4)(PO_4)_2 + K_2M^{VI}O_4$$

It is worth noticing that in the latter scheme $K_2M^{VI}{}_2O_7$ is used due to the equal ratio $K_2M^{VI}O_4$:$M^{VI}O_3$ in the corresponding region. While regions of phosphates crystallization depends of the nature of trivalent metal, the areas with $K_2M^{III}{}_2(M^{VI}O_4)(PO_4)_2$ almost coincide, indicateing the leading role of tetrahedral units in their formation. IR spectra of three compounds exhibit the characteristic stretching bands at 950−1150 cm^{-1} for phosphate and 750−900 cm^{-1} for molybdate (tungstate) tetrahedra.

The maximum content of the molybdate or the tungstate component matches the vitreous areas or Fe_2O_3 recrystallization part (Figure 1). Only in the case of the K−Sc−Mo−O molten system does the single molybdate $KSc(MoO_4)_2$ appear (Figure 2). This fact confirms the low chemical reactivity of $M^{VI}O_4^{2-}$ groups in molten media caused by weaker electrostatic interaction due to a decreased charge and increased size in comparison to PO_4^{3-} ones.

In all, molybdates (tungstates) as a part of a multicomponent solution can play the role of both an inert solution and a direct reactant depending on its concentration. As shown, the area of effective competition between different anionic groups is found under an excess of molybdate component and leads to a new phosphate−molybdate.

Crystallochemical Features of $K_2M^{III}{}_2(M^{VI}O_4)(PO_4)_2$ (M^{III} = Fe, Sc; M^{VI} = Mo, W) Frameworks. Langbeinite-type compounds $A_xB_2(XO_4)_3$ containing sulfate, molybdate, and especially phosphate anions are a structurally well-studied family of solids with several alternative structural descriptions.[10] While considering the simplest building element $[B_2X_3O_{18}]$, which consists of a pair isolated octahedra BO_6 interlinked via three tetrahedral units XO_4, most attention has been given to cationic disorder within two positions B1 and B2. The oxygen surrounding them is characterized by compression of octahedra along the 3-fold axis in such a way that two inner and two outer faces are found to be parallel (Figure 4). The two pairs of planes created through these faces make it possible to distinguish the distances between them as the octahedral thickness value for the polyhedron distortion's evaluation (marked in Figure 4 as d_{oh}^1 and d_{oh}^2). As both positions B1 and B2 in the case of phosphate salts are partially occupied with different polyvalent cations usually with complex preferences, these values were observed to be sensitive to changes of distortion and occupancies.[17] In contrast to previous results the group of langbeinite-related $K_2M^{III}{}_2(M^{VI}O_4)(PO_4)_2$ structures represents a novel type of distortion within the tetrahedral unit XO_4. In spite of having different sizes and oxidation states, phosphorus and molybdenum (tungsten) occupy one unique position with a ratio P/M^{VI} = 2:1. The corresponding tetrahedron is characterized by a set of X−O distances that are a combination of average P−O and M^{VI}−O ones (Table 2).

Applying the scheme proposed in 17 the third distance d_{td} may be considered as a value with the thickness of the tetrahedral group (Figure 4) to study the contribution of P/M^{VI} substitution in structural distortions. In comparison to other related compounds (Figure 5) some important conclusions concerning changes of d values should be pointed out. For all related solids d_{oh}^1 and d_{oh}^2 strongly depend on the nature of metals B1 and B2. Despite having a different metal partner in

Table 3. Magnetic Properties of Langbeinite-Related Iron-Containing Phosphates

compound	Curie−Weiss law region, K	C, emu·K·mol^{-1}	θ_p, K	μ_{eff}	ref
$K_{1.84}Fe_{1.42}Nb_{0.58}(PO_4)_3$	50−300	4.17	−46.25	5.38	18
$K_2Fe_{0.5}Ti_{1.5}(PO_4)_3$	10−300	2.93	−22.14	4.66	20
$K_{11}Fe_{15}O(PO_4)_{18}$	6−300	5.59	−88.39	58.82	23

dx.doi.org/10.1021/ic201575v | Inorg. Chem. 2012, 51, 1380−1385

both positions B, for a set of iron-containing compounds ($K_{1.84}Fe_{1.42}Nb_{0.58}(PO_4)_3$,[18] $K_2FeSn(PO_4)_3$,[19] $K_2Fe_{0.5}Ti_{1.5}(PO_4)_3$,[20] and KFeMo) these values are alike and approach 2.25(6) and 2.21(4) Å correspondingly. The same dependence is observed for scandium-containing ones: $K_2ScSn(AsO_4)_3$[21] and KScMo, KScW.

However, a newly proposed value d_{td} changes significantly with transition from phosphate to other tetrahedral groups. The explanation of this fact lies in the geometrical peculiarities of the XO_4 groups and the framework generally. In the case of mixed $(P/M^{VI})O_4$ anions the longest P/M^{VI}–O bond length (dashed line on Figure 4) links two octahedra from adjacent $[B_2X_3O_{18}]$ fragments, thus elongating the distance between neighboring units and, consequently, loosenong the structure. For P/Mo–O this distance is equal to 1.612(7) Å and P/W–O is 1.620(5) Å (Table 2). The corresponding d_{td} value in both cases approaches that of the AsO_4 group (Figure 5).

To study the stability of the mixed framework obtained in comparison with purely phosphate ones the bond-valence sums (BVSs) were calculated using parameters from ref 22. For partially occupied sites the equation

$$S = \exp((R_o - R)/0.37)$$

was modified including the R_o parameter for the substituted position

$$R_o = R_o(P) \times Oc(P) + R_o(M^{VI}) \times Oc(M^{VI})$$

where $R_o(P)$ and $R_o(M^{VI})$ are bond-valence parameters and $Oc(P)$ and $Oc(M^{VI})$ are the crystallographic occupancies. The mean calculated BVS value for the P/Mo positions in KFeMo and KScMo is 5.77 ± 0.02, and for P/W it is 5.66, which are expected for tetraherally coordinated atoms X taking into account the linear sum of P–O and M^{VI}–O taking into account the corresponding occupancies.

Nevertheless, the corresponding values for B1, B2, A1, and A2 (here countercation A is K: A1 with 9 closest K–O contacts and A2 with 12 ones) positions differ appreciably from the chemical valences. Thus, BVS values for B1/B2 sites are much higher: 3.26 ± 0.01/3.28 ± 0.01 for KFeMo and 3.33 ± 0.02/3.28 ± 0.01 for KScMo and KScW, respectively. Similar deviations of the BVS values from chemical valences have been observed for a number of related compounds and explained by dispersion of the occupancy within these two positions. However, the explanation should be done in light of BVS calculations for potassium sites also. A1 and A2 are usually considered as countercations located in cavities of the framework, but some calculations describing the oxygen environment of K may be done. Eventually BVS values are found to be lower than chemical valences: 0.67 ± 0.05 for K1 and 0.89 ± 0.07. Thus, the general trend of the BVS values of the potassium atom appears to be unreasonable as it was found for cesium atoms in the same type of network. Earlier this fact was explained by the rigidity and tension within the linkage of the comparably small phosphate group and large cations nearby. Substitution by a large tetrahedron was proposed to stabilize the structure with relatively heavy metals.[17] It turns out that partial substitution of P for Mo shows that the tension of the framework does not decrease: the BVS sum of positively charged elements even exceeds the sum of negatively charged O (equal to −24 per formula unit) and is close to +25.39 ± 0.35. This points out the bond redistribution in the framework: Fe–O distances seem to become more covalent and K–O more ionic to meet the requirements of the langbeinite structural type.

Mössbauer Study and Magnetic Properties of KFeMo. The Mössbauer spectrum of KFeMo was recorded at 80 K (Figure 6). It consists of two resonance signals, a well resolved quadrupole doublet with ΔE_Q = 0.54(5) mm s^{-1} and a broadened singlet, possibly an unresolved quadrupole doublet with ΔE_Q = 0.19(3) mm s^{-1}. Both signals have identical values of the isomer shift [δ = 0.58(1) mm s^{-1}] assignable to high-spin Fe^{III} ions. The ratio between the relative areas of the doublets is very near to 1:1, which is in complete agreement with the structural data.

The magnetic susceptibility of KFeMo was measured in the 2–300 K range at 200 Oe using a polycrystalline powder sample (Figure 7). The linear behavior of $\chi_M^{-1}(T)$ above 50 K obeys the Curie–Weiss equation well with a Weiss constant θ = −83.5 K, thus indicating an overall strong antiferromagnetic interaction, as observed for other langbeinite-related compounds (Table 3). The value of $\chi_M T$ at 300 K is 7.73 cm^3 K mol^{-1} and thus less than the spin-only value of 8.76 cm^3 K mol^{-1} expected for two magnetically isolated high-spin Fe^{III} ions. The product $\chi_M T$ first decreases smoothly to a minimum of 2.75 cm^3 K mol^{-1} at 28.0 K, raises rapidly to a maximum of 5.78 cm^3 K mol^{-1} at 20.9 K, and decreases upon further cooling. This behavior resembles the L type of ferrimagnetism described for similar compounds with two inequivalent ferromagnetic sublattices coupled antiferromagnetically through Fe–O–E–O–Fe superexchange pathways (E = S, P, Mo etc.).[24]

CONCLUSIONS

In this work, the great potential of langbeinite structural type to adopt not only different polyvalent metals with different coordination requirements but also tetrahedral groups was demonstrated by 1/3 PO_4^{3-} for MoO_4^{2-} substitution. Three novel representatives of the langbeinite family $K_2Fe(MoO_4)(PO_4)_2$, $K_2Sc(MoO_4)(PO_4)_2$, and $K_2Sc(WO_4)(PO_4)_2$ were isolated from molten phosphate–molybdate salts and characterized by X-ray single-crystal diffraction and IR spectroscopy. For the iron-containing one a Mossbauer study and the magnetic properties were studied. Taking into account bond-valence sum calculations, in particular the calculated valence sum of positively charged elements and geometry of $P/M^{VI}O_4$ species of the whole structure seems to be tense, although structural analysis of synthetic solids appears to evidence a plasticity effect for the langbeinite structure, possibly driven by the structural requirements of the condensed fragment containing two octahedra with three phosphate groups. Introduction of various polyvalent metals in the network causes octahedral distortion, while including different tetrahedral units leads to moving apart the structural fragments, which keep the whole structure stable. These factors may be useful for crystal design of novel functional materials based on this structural type for widening or improving its application areas, for instance, radioactive waste immobilization.

ASSOCIATED CONTENT

Supporting Information

Crystallographic data in CIF format (three files) and IR spectra. This material is available free of charge via the Internet at http://pubs.acs.org.

dx.doi.org/10.1021/ic201575v | Inorg. Chem. 2012, 51, 1380–1385

AUTHOR INFORMATION

Corresponding Author
*E-mail: Tereb@bigmir.net.

ACKNOWLEDGMENTS

The authors want to thank I. O. Fritsky, K. V. Domasevich, and V. I. Ivanenko for technical help and useful discussion. This work was supported by ICDD grant no. 03-02.

REFERENCES

(1) Crennell, S. J.; Cheetham, A. K.; Kaduk, J. A.; Jarman, R. H. *J. Mater. Chem.* **1991**, *1*, 297−298.
(2) Cugat, J.; Sole, R. M.; Carvajal, J. J.; Pujol, M. P.; Mateos, X.; Diaz, F.; Agulio, M. *CrystEngComm* **2011**, *13*, 2015−2022.
(3) Takata, K.; Yamada, I.; Azuma, M; Takano, M.; Shimakawa, Y. *Phys. Rev. B* **2007**, *76*, 024429.
(4) Zhang, K.; Zhang, H. *Chin. Sci. Bull.* **1998**, *43*, 529−536.
(5) Sorokina, N. I.; Voronkova, V. I. *Crystallogr. Rep.* **2007**, *52*, 80−93.
(6) Long, Y.; Shimakawa, Y. *New J. Phys.* **2010**, *12*, 063029.
(7) Dambournet, D.; Belharouak, I.; Amine, K. *Inorg. Chem.* **2010**, *49*, 2822−2826.
(8) Piriou, B.; Elfakir, A.; Quarton, M. *J. Lumin.* **2001**, *93*, 17−26.
(9) Norberg, S. T. *Acta Crystallogr.* **2002**, *B58*, 743−749.
(10) Orlova, A. I.; Koryttseva, A. K.; Loginova, E. E. *Radiochemistry* **2011**, *53*, 51−62.
(11) Oelkrug, H.; Brückel, T.; Hohlwein, D.; Hoser, A.; Prandl, W. *Phys. Chem. Miner.* **1988**, 246−249.
(12) Benmoussa, A.; Borel, M. M.; Grandin, A.; Leclaire, A.; Raveau, B. *J. Solid State Chem.* **1992**, *97*, 314−318.
(13) Shpanchenko, R. V.; Lapshina, O. A.; Antipov, E. V.; Hadermann, J.; Kaul, E. E.; Geibel, C. *Mater. Res. Bull.* **2005**, *40*, 1569−1576.
(14) Sheldrick, G. M. *Acta Crystallogr.* **2008**, *A64*, 112−122.
(15) Terebilenko, K. V.; Zatovsky, I. V.; Slobodyanik, N. S.; Domasevitch, K. V.; Pushkin, D. V.; Baumer, V. N. *J. Solid State Chem.* **2007**, *180*, 3351−3359.
(16) Lajmi, B.; Hidouri, M.; Ben Amara, M. *Acta Crystallogr.* **2002**, *C58*, i156−i158.
(17) Ogorodnyk, I. V.; Baumer, V. N.; Zatovsky, I. V.; Slobodyanik, N. S.; Shishkin, O. V.; Domasevitch, K. V. *Acta Crystallogr.* **2007**, *B58*, 819−827.
(18) Babaryk, A. A.; Zatovsky, I.,V.; Slobodyanik, N., S.; Ogorodnyk, I. V. *Z. Naturforsch.* **2008**, *63b*, 345−348.
(19) Zatovsky, I. V.; Yatskin, M. M.; Baumer, V. N.; Slobodyanik, N. S.; Shishkin, O. V. *Acta Crystallogr.* **2007**, *E63*, i199−i199.
(20) Ogorodnyk, I. V.; Zatovsky, I. V.; Baumer, V. N.; Slobodyanik, N. S.; Shishkin, O. V.; Vorona, I. P. *Z. Naturforsch.* **2008**, *63b*, 261−266.
(21) Harrison, W. T. A. *Acta Crystallogr.* **2010**, *C66*, i82−i84.
(22) Brown, I. D.; Altermatt, D. *Acta Crystallogr.* **1985**, *B41*, 244−247.
(23) Lajmi, B.; Hidouri, M.; Wattiaux, A.; Fournes, L.; Darriet, J.; Ben Amara, M. *J. Alloys Compd.* **2003**, *361*, 77−83.
(24) Ouerfelli, N.; Guesmi, A.; Molinie, P.; Mazzac, D.; Zida, M. F.; Driss, A. *J. Solid State Chem.* **2007**, *180*, 3342−2949 and references therein.